REPORT NO. NADC-89046-60

QUENCH SENSITIVITY IN Al-Cu-Li ALLOYS

Mary E. Donnellan and Dr. William E. Frazier
Air Vehicle and Crew Systems Technology Department (Code 6063)
NAVAL AIR DEVELOPMENT CENTER
Warminster, PA 18974-5000

14 FEBRUARY 1989

FINAL REPORT
Period Covering 1 October 1988 to 1 October 1989
Task No. N0001488WX4BS08
Work Unit No. ZP 180
Program Element No. 62234N
Project No. RS34A50

Approved for Public Release; Distribution is Unlimited

Prepared for
Air Vehicle and Crew Systems Technology Department (Code 60C)
NAVAL AIR DEVELOPMENT CENTER
Warminster, PA 18974-5000

NOTICES

REPORT NUMBERING SYSTEM - The numbering of technical project reports issued by the Naval Air Development Center is arranged for specific identification purposes. Each number consists of the Center acronym, the calendar year in which the number was assigned, the sequence number of the report within the specific calandar year, and the official 2-digit correspondence code of the Command Officer or the Functional Department responsible for the report. For example: Report No. NADC 88020-60 indicates the twentieth Center report for the year 1988 and prepared by the Air Vehicle and Crew Systems Technology Department. The numerical codes are as follows:

CODE	OFFICE OR DEPARTMENT
00	Commander, Naval Air Development Center
01	Technical Director, Naval Air Development Center
05	Computer Department
10	AntiSubmarine Warfare Systems Department
20	Tactical Air Systems Department
30	Warfare Systems Analysis Department
40	Communication Navigation Technology Department
50	Mission Avionics Technology Department
60	Air Vehicle & Crew Systems Technology Department
70	Systems & Software Technology Department
80	Engineering Support Group
90	Test & Evaluation Group

PRODUCT ENDORSEMENT - The discussion or instructions concerning commercial products herein do not constitute an endorsement by the Government nor do they convey or imply the license or right to use such products.

APPROVED BY: W F Moroney

W. F. MCPONEY
CAPT, MSC, U.S. NAVY

DATE: 18 Aug 1989

UNCLASSIFIED

SECURITY CLASSIFICATION OF THIS PAGE

REPORT DOCUMENTATION PAGE

Form Approved
OMB No. 0704-0188

1a REPORT SECURITY CLASSIFICATION Unclassified	1b RESTRICTIVE MARKINGS
2a SECURITY CLASSIFICATION AUTHORITY	3 DISTRIBUTION/AVAILABILITY OF REPORT Approved For Public Release. Distribution is Unlimited
2b DECLASSIFICATION/DOWNGRADING SCHEDULE	
4 PERFORMING ORGANIZATION REPORT NUMBER(S) NADC-89046-60	5 MONITORING ORGANIZATION REPORT NUMBER(S)
6a NAME OF PERFORMING ORGANIZATION Air Vehicle and Crew Systems Technology Department 6b OFFICE SYMBOL (If applicable) 6063	7a NAME OF MONITORING ORGANIZATION
6c ADDRESS (City, State, and ZIP Code) NAVAL AIR DEVELOPMENT CENTER Warminster, PA 18974-5000	7b ADDRESS (City, State, and ZIP Code)
8a NAME OF FUNDING/SPONSORING ORGANIZATION Airborne Materials Block 8b OFFICE SYMBOL (If applicable) 60C	9 PROCUREMENT INSTRUMENT IDENTIFICATION NUMBER
8c ADDRESS (City, State, and ZIP Code) NAVAL AIR DEVELOPMENT CENTER Warminster, PA 18974-5000	10 SOURCE OF FUNDING NUMBERS PROGRAM ELEMENT NO: 62234N PROJECT NO: RS34A50 TASK NO: N0001488WX 4BS08 WORK UNIT ACCESSION NO: ZP180
11 TITLE (Include Security Classification) Quench Sensitivity In Al-Cu-Li Alloys	
12 PERSONAL AUTHOR(S) Mary E. Donnellan and Dr. William E. Frazier, Ph.D.	
13a TYPE OF REPORT FINAL 13b TIME COVERED FROM 10/1/88 TO 10/1/89	14 DATE OF REPORT (Year, Month, Day) 1989 February 14 15 PAGE COUNT 28
16 SUPPLEMENTARY NOTATION	

17 COSATI CODES		
FIELD	GROUP	SUB-GROUP
11	06	
11	06 11	

18 SUBJECT TERMS (Continue on reverse if necessary and identify by block number)
2090 Aluminum
Cooling Profiles
Quench Sensitivity
Ti (Al_2CuLi_3)

19 ABSTRACT (Continue on reverse if necessary and identify by block number)

A study has been performed to characterize the quench sensitivity of an aluminum-copper-lithium alloy, 2090. The mechanical properties were evaluated from samples subjected to different quench conditions and heat treatments. Transmission electron microscopy (TEM) was used to examine the microstructural characteristics of the alloy. The results are described with respect to correlations between microstructural characteristics and strength. A range for the critical quench rate of alloy 2090 has been established. The effect of quench sensitivity on hardness and conductivity is also discussed.

20 DISTRIBUTION/AVAILABILITY OF ABSTRACT ☒ UNCLASSIFIED/UNLIMITED ☐ SAME AS RPT ☐ DTIC USERS	21 ABSTRACT SECURITY CLASSIFICATION Unclassified
22a NAME OF RESPONSIBLE INDIVIDUAL Mary E. Donnellan	22b TELEPHONE (Include Area Code) (215) 441-2151 22c OFFICE SYMBOL 6063

DD Form 1473, JUN 86 *Previous editions are obsolete*

S/N 0102-LF-014-6603

SECURITY CLASSIFICATION OF THIS PAGE
UNCLASSIFIED

CONTENTS

FIGURES

TABLES

THIS PAGE INTENTIONALLY LEFT BLANK

INTRODUCTION

Aluminum-lithium alloys are of great interest to the aerospace industry because of their high specific properties. A commercial aluminum-lithium alloy, designated 2090, has been produced for applications requiring high strength. This alloy has a higher modulus (79.4GPa) and lower density ($2.60 gcm^{-3}$) compared to currently used aluminum alloys, e.g., 7075. However, in thick sections, the alloy has poor short transverse fracture toughness, viz., 10MPa $m^{0.5}$ [1].

It is well established that the mechanical, physical, and corrosion behavior of age-hardening aluminum alloys are affected by quench rate [2-5]. The poor through thickness toughness of alloy 2090 can, in part, be attributed to an inadequate quench rate. An inadequate quench rate causes a decrease in vacancy concentration and a decrease in the extent of metastable solute solubility. Together, these two factors reduce microstructural uniformity by increasing the width of precipitate free zones (pfz) and increasing the volume fraction of deleterious grain boundary precipitates [6].

Alloys, such as 2090, in which optimal properties are difficult to obtain using conventional commercial quench practices are typically considered quench sensitive. However, no universally accepted definition of quench sensitivity exists. This investigation examines the quench sensitivity of alloy 2090 in a quantitative manner. Cooling profiles for a number of quenchants and specimen geometries were generated. Specimen quench rate was correlated to mechanical properties and microstructure.

THIS PAGE INTENTIONALLY LEFT BLANK

EXPERIMENTAL PROCEDURE

MATERIAL

Alloy 2090 was procured from ALCOA in the form of cross-rolled 1.27 cm and 3.81 cm thick plate. Rectangular bars, (5.08 cm X 1.27 cm X 20.32 cm) and (5.08 cm X 3.81 cm X 20.32 cm), were machined from each plate, respectively.

COOLING PROFILES

Iron-constantine thermocouples were imbedded in the center of each specimen in order to monitor the cooling rate for each quench condition. The bars were solution heat treated at 550°C for 30 minutes and quenched in one of four different media: 1) ice brine (-4°C), 2) room temperature water (20°C), 3) hot water (80°C), and 4) ambient temperature air. The 1.27 cm bars were quenched in room temperature water (20°C). The quench rate profiles were recorded using an analogue output interfaced with an ITT personal computer utilizing appropriate software, LabTech Notebook™. The cooling rates were recorded at the center of each plate. Ten temperature readings were recorded per second.

THERMAL MECHANICAL TREATMENT

All of the samples were stretched 6% after quenching and prior to artificial aging. Tensile specimens were machined from the stretched material and then aged 8 hours at 190°C. Samples were examined in both the as-quenched and artificially aged conditions.

MICROSTRUCTURAL CHARACTERIZATION

The microstructures of the alloys were examined using optical and transmission electron microscopy (TEM). The TEM specimens were prepared using a Struers Tenupole twin jet electropolisher in a 1:4 nitric acid:methanol solution held at a constant -20°C. All specimens were thinned at a 12 V potential and 1.5 amp current. The TEM examination of the specimens was performed using a JEOL 100 CX II at 120 kV. The as-quenched and aged microstructures were examined to identify changes in the precipitate size, distribution, and morphology. Samples were studied in the as-quenched and stretched condition, and in the unstretched condition. Dark field TEM was used to image the T1 precipitates using their [112] zone axis reflections.

MECHANICAL PROPERTIES

The hardness and tensile response of the alloys were measured and correlated with microstructural features. Tensile tests were performed using a MTS loading apparatus at a strain rate of 2.5×10^{-3} cm/s. 0.640 cm diameter tensile samples were made and tested according to ASTM specification B557.

Hardness (Rockwell B) measurements were taken using a Wilson hardness tester model 3JR. Hardness was measured as a function of aging time at 190°C in the stretched condition. Samples were 2.54 cm X 2.54 cm X 1.27 cm with a polished surface.

FRACTOGRAPHY

The fracture surfaces of the tensile samples were examined using an Amray scanning electron microscope (SEM) Model 1000B Fractographs were produced by secondary electron imaging.

CONDUCTIVITY

Electrical conductivity was measured in units of percent internationally accepted copper standard (%IACS) on a Forster Sigmatest, Model 2.067. The conductivity of the stretched specimens was measured as a function of their aging time at 190°C. Samples were 2.54 cm X 2.54 cm X 1.27 cm with a polished surface.

RESULTS

MATERIAL

Optical microstructures of the 1.27 cm and 3.81 cm plates are presented in Figures 1a and 1b. The grains were "pan-caked" shaped with the longest dimension in the rolling direction. The average grain size for the 1.27 cm plate is 12.5 um X 75 um X 50 um. The average grain size for the 3.81 cm plate is 37.5 um X 100 um X 50 um. The compositions of the 1.27 cm and 3.81 cm thick plates were determined by wet chemical analysis, see Table 1.

COOLING PROFILES

The cooling profiles for the various quench conditions are given in Figure 2. As expected, as the temperature of the quenchant and/or thickness of the bar increased, the specimen's cooling rate decreased. In this study, the specimen's quench rate is defined as the slope of the tangent to the cooling curve measured between 500°C and 275°C. These values are given in Table 2. The quench rates for the 1.27 cm bar in the room temperature water and the hot water quenchants were approximately the same, i.e., 47°C/sec. The ice brine solution had a significantly faster quench rate (85°C/sec), and the air cool demonstrated a significantly slower quench rate (0.5°C/sec). The 3.81 cm bar quenched in room temperature water exhibited a quench rate intermediate between the 1.27 cm bar in hot water and air, i.e., 36°C/sec. Throughout this paper the water cooled 3.81 cm plate and the air cooled 1.27 cm plate are referred to as "slow quenched" samples; all other samples are referred to as "fast quenched" samples.

As Quenched Condition

In the as quenched and stretched condition, the solid solution, delta prime (coherent Al_3Li), and beta phases (Al_3Zr) were present in both the slow and fast quenched samples. The primary difference between the slow and fast quenched samples was the presence of the T1 phase in the slow quenched samples, (Figure 3a & 3b). In the air cooled and stretched condition the T1 phase was measured to be as large as 2 um in length. In the 3.81 cm plate the T1 phase was an average of 0.4 um in length. The T1 phase was detected primarily along the subgrain and grain boundaries. The diameter of the beta particles were approximately 0.04 um in both slow quenched samples. The delta prime phase was too fine to measure, (Figure 4). Also, the slow cooled samples displayed an unidentified grain boundary precipitate during the quench, Figure 5. This phase was not as ubiquitous as the T1 phase. The particles were small, approximately 0.35 um in diameter.

In the as quenched condition, the fast quenched material was comprised of the solid solution, delta [illegible] and beta phases. The beta phase was approximately 0.04 um in diameter. There were no other [illegible]es present.

Aged Condition

After aging at 190°C for 8 hours, differences in the microstructures of the slow cooled and fast quenched samples were also observed. The slow cooled, stretched, and aged material displayed the delta prime, beta, T1 and other unidentified grain boundary phases. The T1 phase was larger after aging. The length of the T1 phase in the air cooled samples was as large as 3 um and it was primarily located along the subgrain and grain boundaries, Figure 6a. The delta prime phase also was larger. The diameter was approximately 0.03 um, and it was homogeneously distributed throughout the grains, Figure 6b. The beta phase was approximately 0.06 um in diameter and appears to be coated with delta prime. The unidentified grain boundary phases were still present in the aged condition.

a)

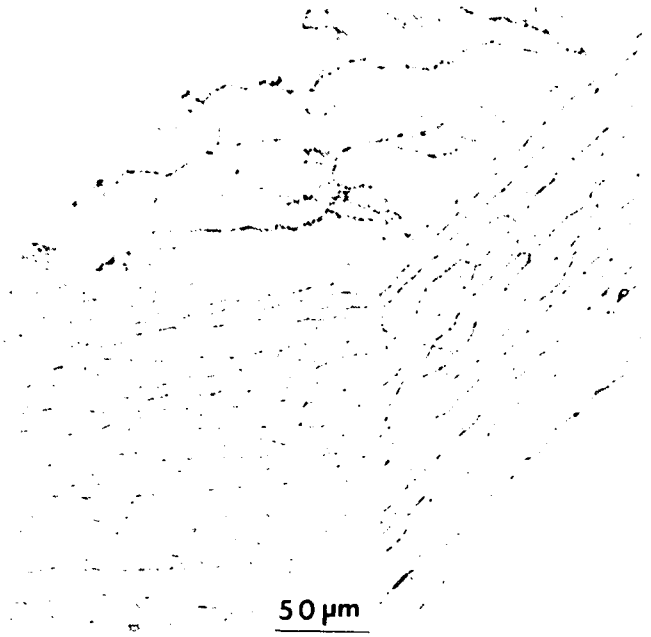

b)

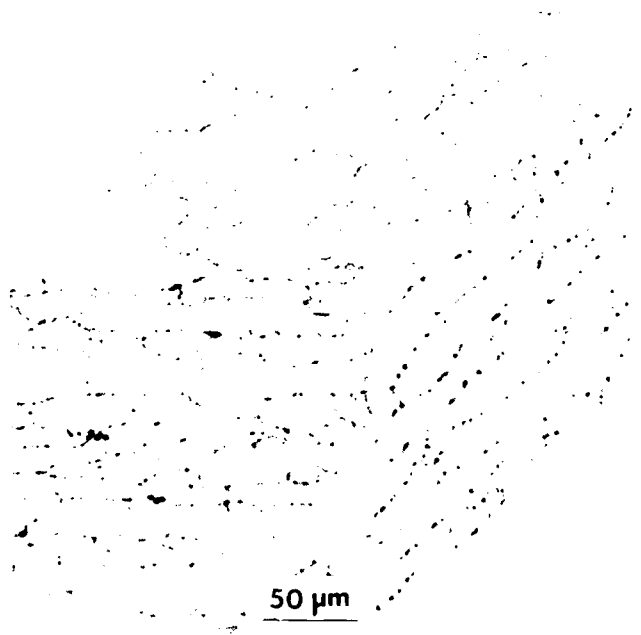

Figure 1. Optical Micrographs, 2090 plate etched with Keller's Reagent.
a) 1.27 cm (.5") thick
b) 3.81 cm (1.5") thick

Table 1. Composition 2090 Plate (Wt. %)

Alloy	Cu	Li	Mg	Zr	Fe	Si
2090 Range	2.4 - 3.0	1.9 - 2.6	0.25	.08 - .15	0.10	0.12
* 2090 .5" (1.27 cm) Plate	2.60	1.96	.001	.110	.016	.060
* 2090 1.5" (3.81 cm) Plate	3.20	2.10	.01	.08	.40	.13

* Taken from Center of Plate after SHT 550°C for 30 Minutes

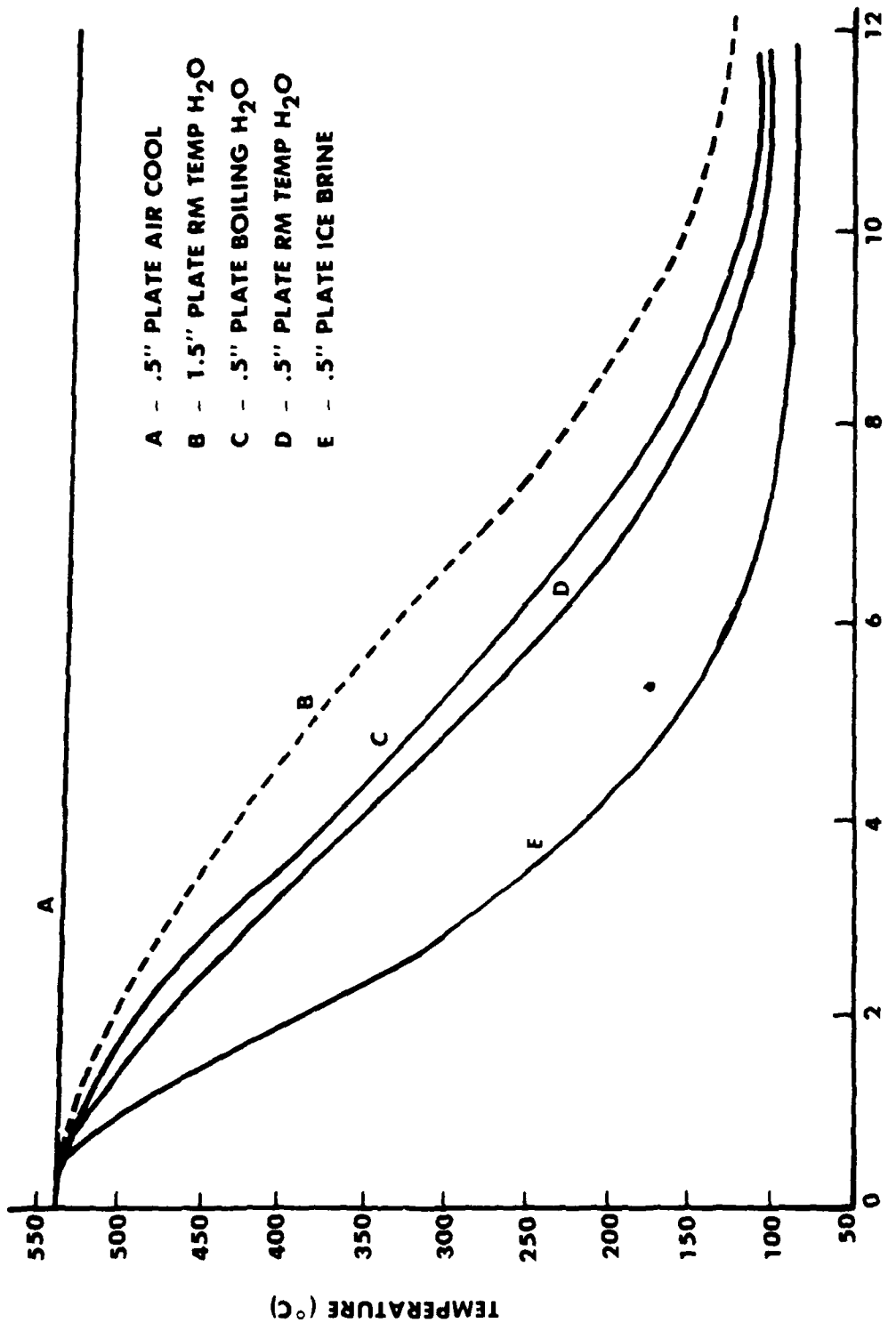

Figure 2. Cooling Profiles During Quench, 2090 Plate

Table 2. Cooling Rate at Center of Plate (500°C to 275°C)

Sample	Rate (°C/Sec)
A	0.5
B	36
C	46
D	48
E	85

Figure 3. Alloy 2090, Slow quenched conditions A and B. Dark Field TEM micrograpgh of the T_1 Phase.
a) Sample A
b) Sample B

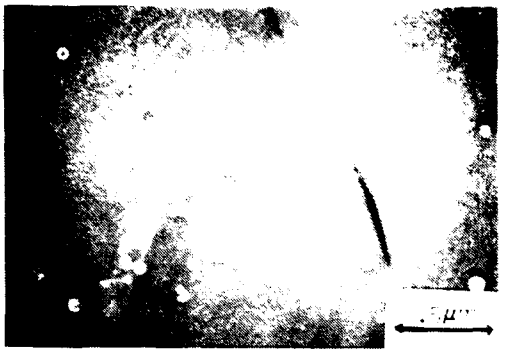

Figure 4. Alloy 2090, Slow quenched condition A. Dark Field TEM micrograph of the Al_3 Li Phase.

Figure 5. Alloy 2090, Slow quenched condition B. Bright Field TEM micrograph of an unidentified grain boundary precipitate.

The fast quenched, stretched, and aged samples displayed the solid solution, delta prime, beta and T1 phases in the aged condition. The length of the T1 phase was approximately 0.19 um. The T1 phase was distributed uniformly throughout the matrix as well as along the grain boundaries. The size of the T1 phase was much smaller along the grain boundaries than in the slow cooled material, Figure 7a. The diameter of the delta prime particles was approximately 0.02 um. The diameter of the beta was approximately 0.06 um. The beta phase may be coated with delta prime here also, Figure 7b.

MECHANICAL PROPERTIES

Tensile data are given in Table 3. In the as-quenched conditions, the ultimate tensile strengths (UTS) range from 312 to 349 MPa and the yield strengths (YS) range from 128 to 162 MPa. The ductility, percent elongation, for the fast quenched samples is between 16-18%, but for the slowly quenched samples is 2-12%. The slow quenched samples show lower ductility due to precipitation during the slow quench.

In the as-quenched condition, the air cooled samples exhibit the highest yield strength, 162 MPa. This is due to precipitation of strengthening phases during the quench. The fast quenched samples had an average yield strength of 137 MPa. This is a significant difference, 25 MPa. It is expected that the other slow quenched samples, the 3.81 cm thick plate water cooled, would exhibit a high yield strength similar to the air cooled samples. This is not the case. The 3.81 cm plate, water quenched, showed the lowest yield strength, 128 MPa. This may be due to differences in composition, texture or amount of stretch between the 3.81 cm and 1.27cm thick plates. The thicker plate may not have experienced a full 6% stretch through the thickness.

In the aged condition, the ultimate tensile strengths, yield strengths, and elongations were much higher for the fast quenched samples than the slow quenched samples. The fast quenched samples exhibited yield strengths ranging from 526 MPa to 535 MPa and elongations from 7 to 9%. The air cooled samples exhibited a lower yield strength, 448 MPa, and lower elongations (5%). The yield strength of the 3.81 cm plate was the lowest, 476 MPa. The ice brine quenched samples consistently showed the highest yield strengths. It follows from the tensile data that the strength and ductility in the aged conditions are higher with the faster quench rates.

The hardness (Rb) as a function of age time at 190°C is given in Figure 8. A significant difference in hardness is exhibited between the slow quenched samples and the fast quenched samples. In the as-quenched condition the hardness of the slow quenched sample is high due to the precipitation of a significant amount of precipitate phases during the quench. After approximately 40 minutes aging at 190°C the faster quenched alloys exhibit a higher hardness which continues up to 200 hours age time. The hardness of the air cooled samples is lower after 40 minutes age time due to the coarsening of the precipitates which were formed during the quench and the precipitation of equilibrium phases during longer aging times. These phases are present along the grain boundaries and sub grain boundaries.

FRACTOGRAPHY

The fractographs obtained using SEM displayed significant differences between the alloys due to the differences in quench rate. The alloys which were fast quenched, stretched 6% and tested, displayed predominantly shear type fracture behavior. This is apparent from the smooth fracture surface at a 45 angle from the loading axis, (Figures 9a and 9b). The alloys which were slow cooled, stretched 6% and tested displayed a very jagged fracture surface, (Figures 10a and 10b). After aging for 8 hours at 190°C, all of the alloys displayed a jagged predominantly transgranular fracture surface. However, the samples which had been slow cooled had extreme cracking parallel to the loading direction which was not apparent in the fast quenched alloys, Figures 11a, 11b, 12a, and 12b.

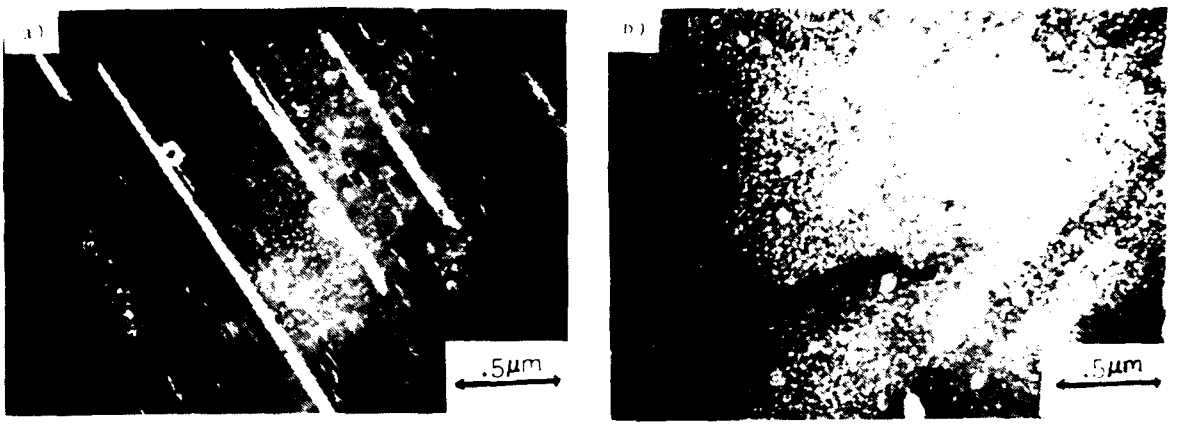

Figure 6. Alloy 2090, Slow quenched condition A. Stretched 6%, Aged 8 hours at 190° C.
a) Dark Field T_1 phase
b) Dark Field Al_3 Li phase

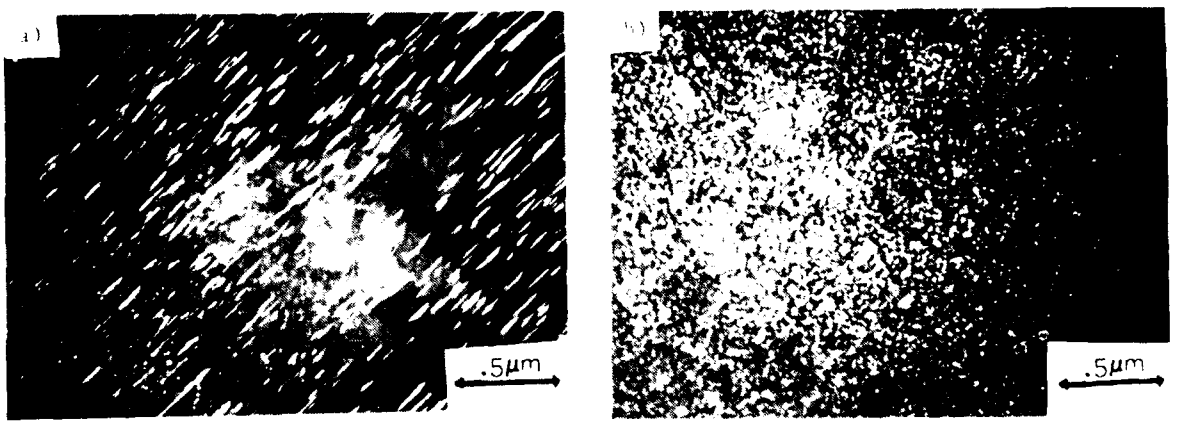

Figure 7. Alloy 2090, Fast quenched condition E. Stretched 6%, Aged 8 hours at 190°C.
a) Dark Field T_1 phase
b) Dark Field Al_3 Li phase

Table 3. Tensile Data*, Alloy 2090

	Slow Quenched		Fast Quenched		
Condition As-Quenched					
Sample	**A**	**B**	**C**	**D**	**E**
Y.S. (MPa)	162	128	138	139	135
U.T.S. (MPa)	334	312	331	331	349
% Elongation	2	12	16	17	19
Condition 6% Stretch and Aged 8 Hours at 190°C					
Sample	**A**	**B**	**C**	**D**	**E**
Y.S. (MPa)	448	338	530	526	535
U.T.S. (MPa)	513	476	570	570	575
% Elongation	5	6	9	7	7

*Data Are Average of 4 Specimens

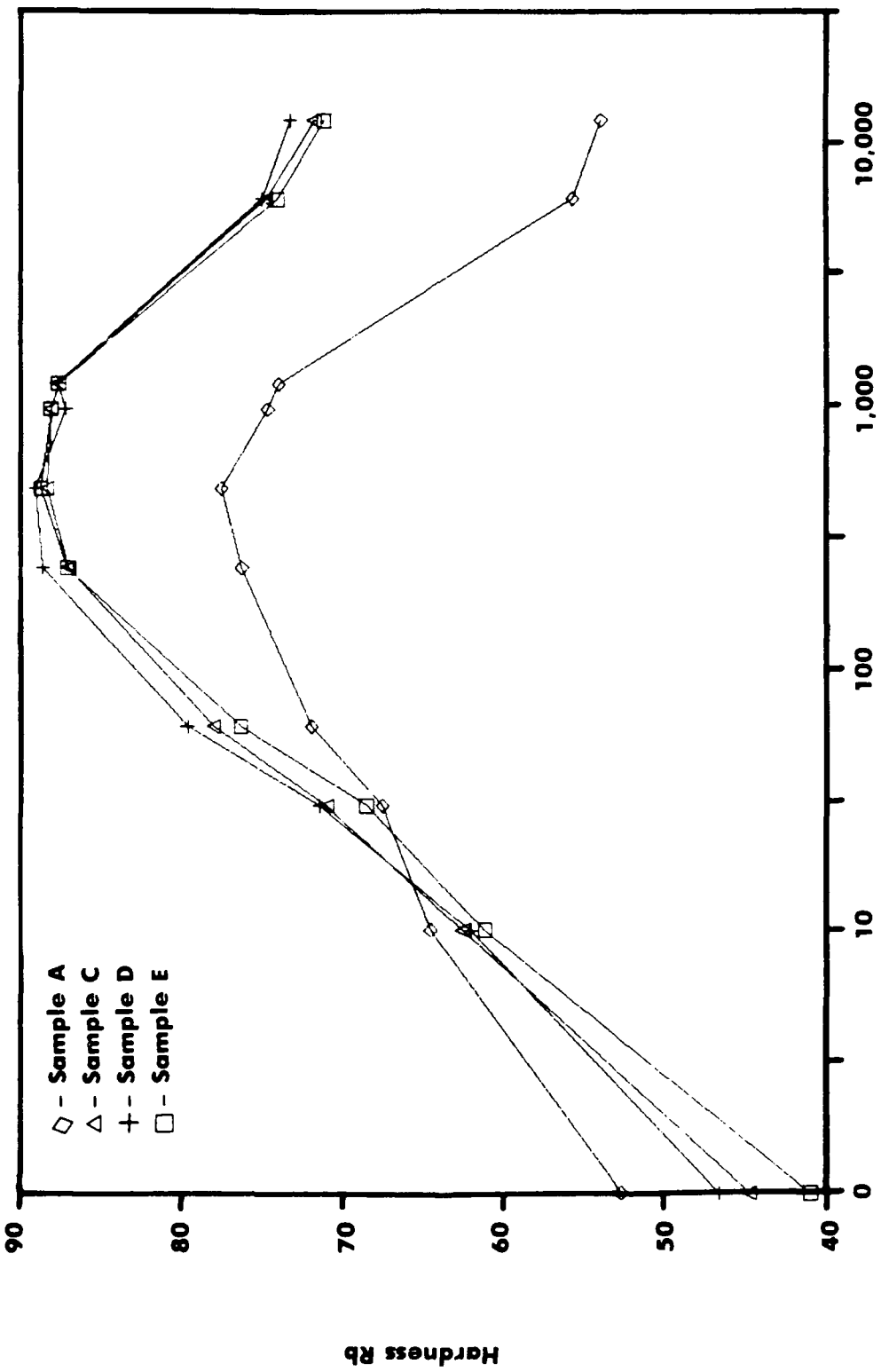

Figure 8. Hardness vs. Age Time at 190°C, 2090 .5" Plate

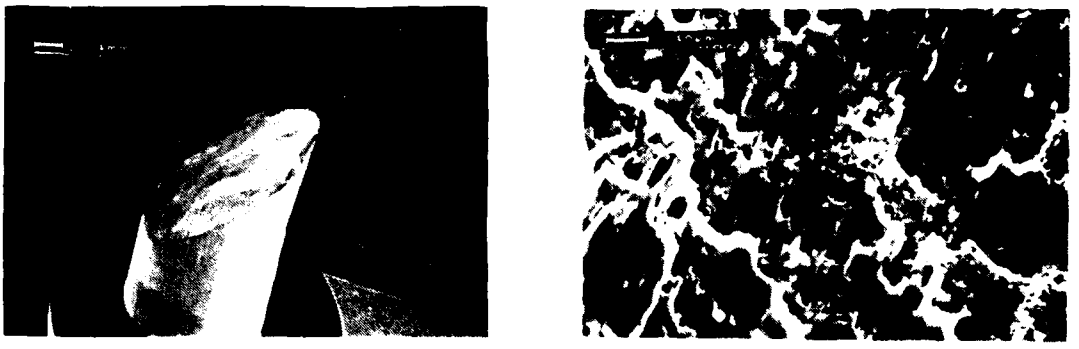

Figure 9. SEM micrographs display fracture surface from sample E in the as-quenched condition. a) 7X b) 1000X

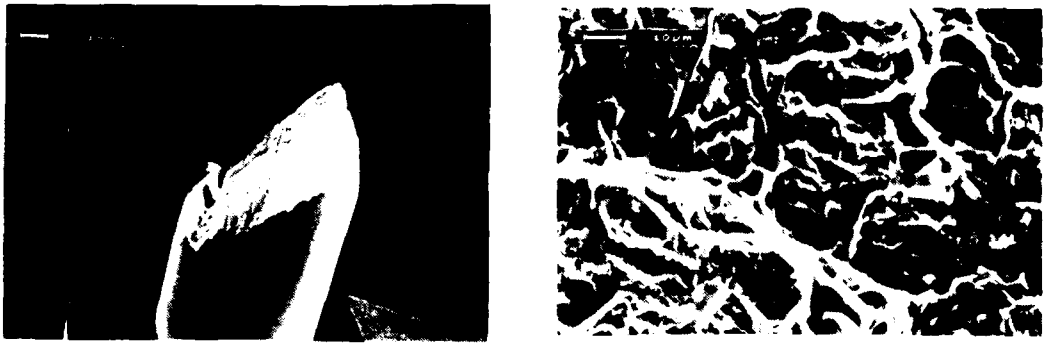

Figure 10. SEM micrographs display fracture surface from sample A in the as-quenched condition. a) 7X b) 1000X

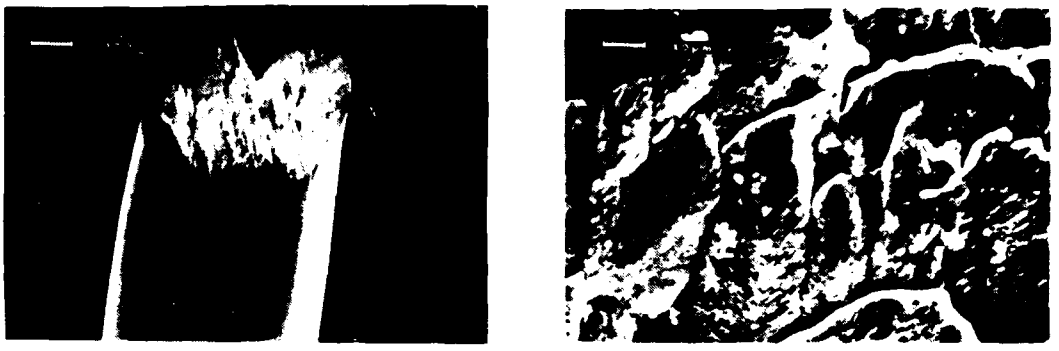

Figure 11. SEM micrographs display fracture surface from sample E aged 8 hours at 190°C. a) 7X b) 1000X

Figure 12. SEM micrographs display fracture surface from sample A aged 8 hours at 190°C. a) 7X b) 1000X

CONDUCTIVITY

The conductivity (%IACS) as a function of aging time at 190°C is given in Figure 13. All quench conditions exhibit an initial increase in conductivity followed by a decrease and a final increase. Once again, the slow cooled sample exhibits significantly different behavior than the other three conditions. The conductivity of the slow cooled sample remains lowest through 100 hours age time at 190°C.

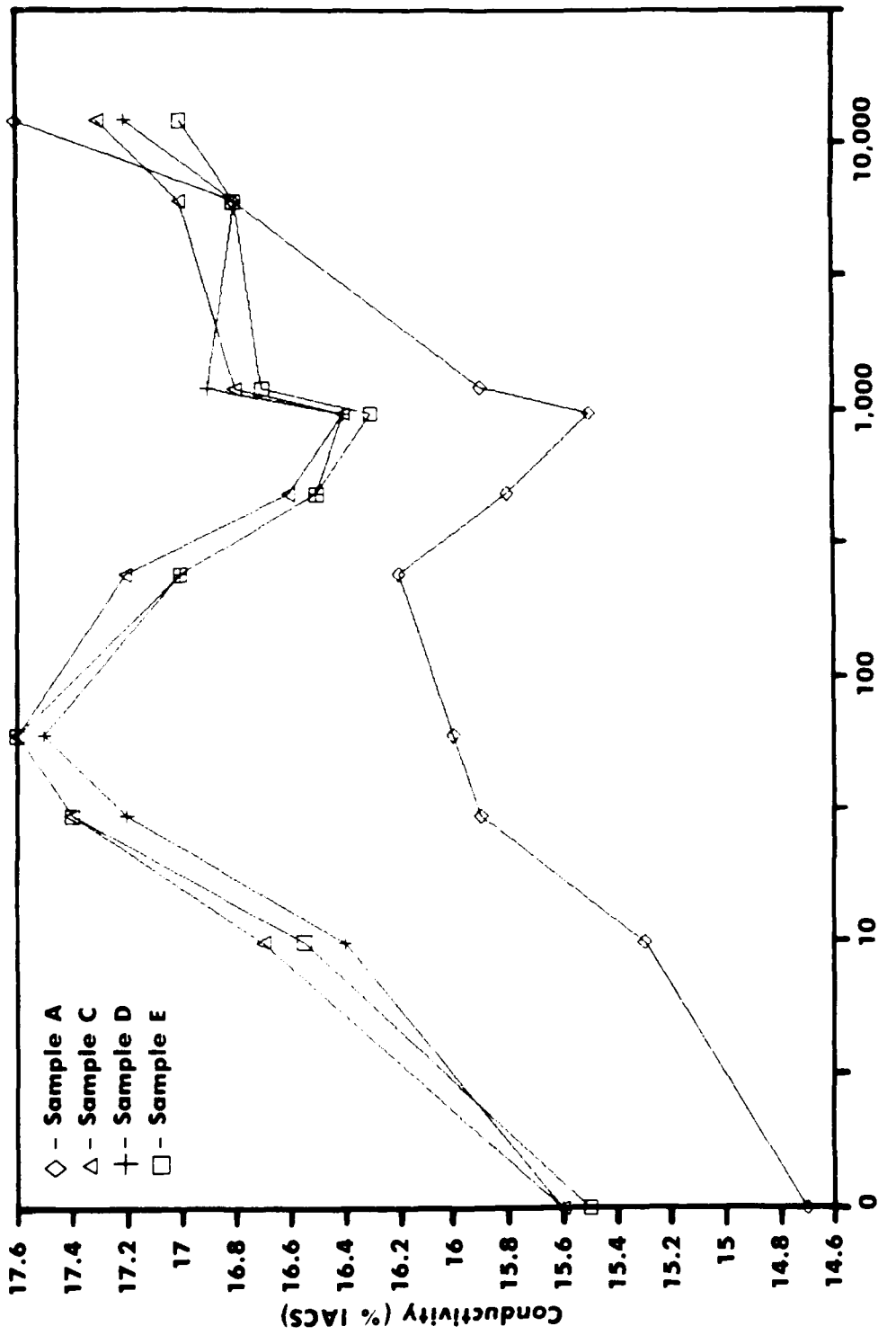

Figure 13. Conductivity vs. Age Time at 190°C, 2090 .5" Plate

DISCUSSION

The discussion is divided into four separate categories. The effect of quench rate on the following: (1) microstructure; (2) mechanical properties; (3) fractography; and (4) conductivity.

MICROSTRUCTURE

The TEM examination of the microstructures in the as-quenched conditions shows subtle differences between the fast quenched samples and the slow quenched samples. As described in the results, there are variations in the types of precipitates present, the size of the precipitates and their distribution.

There was not a noticeable difference in the size of the delta prime phase due to differences in the quench rate in the as quenched condition. There was not a discernible change in the dispersoid phase, Al_3Zr, due to varying the quench rate. The dispersoid phase had the same size and distribution regardless of the quench rate experienced. The only significant difference in the as quenched condition was the presence of grain boundary precipitates in the slow quenched samples. The presence of these grain boundary precipitates, primarily the T1 phase, is the cause of the quench sensitivity in alloy 2090.

The slow quenched samples precipitated large platelets of T1 along the subgrain and grain boundaries during the quench. This was observed in the air cooled sample and the 3.81 cm plate sample. The slow cooled samples also showed grain boundary precipitates in addition to the T1 phase during the quench. These grain boundary precipitates may be the metastable T2 phase or the equilibrium delta phase. These phases have been previously identified in this alloy system at longer aging times.[7] However, these grain boundary precipitates were not present in large amounts in the slow quenched samples. The T1 phase was the predominant grain boundary precipitate. The T1 phase appears to have a lower energy barrier to nucleation than other grain boundary precipitates. Therefore, T1 precipitates more readily during a slow quench. T1 is the primary grain boundary precipitate in this alloy during slow quenching. The formation of grain boundary precipitates during slow quenching must be avoided in order to attain the optimum mechanical properties.

After aging there are significant changes in the microstructure due to varying the quench rate. After aging, the dispersoid phase was the same size. However, the delta prime phase was larger in the slow cooled material, and there were changes in the size and distribution of the T1 phase. The T1 precipitates which formed along the subgrain and grain boundaries during the slow quench grew upon aging and caused brittle fracture. In the fast quenched alloys the quench rate was fast enough to avoid grain boundary precipitation during the quench. Hence, the T1 phase was able to nucleate on dislocations throughout the matrix during aging. The resulting T1 precipitates were smaller in size and more uniformly distributed throughout the matrix in the fast quenched samples. This contributed to improved mechanical properties.

The critical quench rate as defined in this study as the maximum cooling rate which can be experienced without precipitation of deleterious grain boundary precipitates during the quench. Therefore, it is established that the quench rates for 1.27 cm thick plate in the ice brine, room temperature and hot water quenches exceed the critical quench rate. The data indicate that the critical quench rate is slower than 46°C/s.

MECHANICAL PROPERTIES

The different microstructures, due to variation of the quench rate, have a significant effect on the subsequent mechanical properties. In the as-quenched condition the UTS and YS is highest for the air cooled samples. This is due to the presence of strengthening precipitates, delta prime and T1. However,

the ductility (% elongation) is lowest in the air cooled samples. This is due to the precipitation of the T1 phase and precipitates along the grain boundaries during the slow cooling process. The 3.81 cm plate water quenched samples show the lowest UTS and YS. This is unexpected since the cooling rate was slow and T1 grain boundary precipitates precipitated during the quench. However, the low yield strength may be attributed to a difference in composition, texture or amount of stretch between the 1.27 cm thick plate and the 3.81 cm thick plate. Due to the increased thickness the 6% stretch may not have been achieved through the entire thickness of the plate. A lower amount of stretch would contribute to a decrease in strength after aging.

There is not a significant difference in UTS or YS strength levels among the fast quenched samples in the as-quenched condition. They are lower than the air cooled samples due to a lack of strengthening phases. Also, the ductility levels of the fast quenched alloys were similar and greater than the air cooled samples for the same reason.

In the 8-hour aged condition, the mechanical properties exhibited a greater variation due to quench rate than in the as-quenched condition. The slow quenched samples had the lowest strength and ductility values. This is due to the growth of large platelets of T1 along the subgrain and grain boundaries and less precipitation within the grains. Conversely, the fast quenched samples exhibited adequate strength and ductility after stretching and aging. Sufficient solute was retained in the matrix during the fast quench so that precipitation of strengthening phases occurred more uniformly through out the grains during aging. The presence of a more uniform distribution of the T1 phase is responsible for the improvement in strength.

Upon aging at 190°C both the slow quenched and fast quenched samples show the same trend in hardness. Initially the hardness increases due to the precipitation of the delta prime and T1 phases. Up to 16 hours aging time the slow quenched samples have a higher hardness because more precipitation has occurred. However, eventually the slow quenched samples grow very large coarse precipitates, whereas the fast quenched samples have many uniformly distributed smaller precipitates. Hence, the hardness of the fast quenched samples exceeds the slow quenched samples. At longer aging times the hardness for both the slow and fast quenched samples decreases due to concurrent precipitate coarsening and additional grain boundary precipitation.

FRACTOGRAPHY

It is significant to note that all of the fracture surfaces of the fast quenched samples were a smooth 45 degree fracture from the loading axis. This indicates a predominantly transgranular shear type of fracture. This agrees well with the fact that the delta prime is a shearable precipitate. This is the only precipitate which was observed in this condition. The fracture surfaces of the slow quenched samples were very jagged. This indicates a predominantly intergranular fracture due to the presence of grain boundary precipitates. The T1 phase is non-shearable, and therefore, would promote a intergranular type fracture. This agrees well with the microstructural observations that the T1 phase is present in this condition.

CONDUCTIVITY

The conductivity increases up to approximately one and a half hours of aging time. It is expected that as solute atoms are removed from the matrix, such as when precipitation of a second phase occurs, the conductivity will increase. The conductivity of 2090 increases up to 60 minutes aging time at 190°C due to the precipitation of delta prime and T1. The conductivity then decreases. This attributed to an increase in strain between the precipitate and matrix as the precipitates grow. An increase in the strain field with the matrix may contribute to impeding electron movement, and therefore, decreasing the electrical

conductivity. The minimum in conductivity which occurs at approximately 1000 minutes aging time is due to a competition between coherency strain which impedes electron movement and increasing solute depletion which aides electron movement. After 1000 minutes aging the conductivity increases. At longer aging times, there is precipitation of the delta and T2 phases. The conductivity increases due to further depletion of solute from the matrix and a decrease in the strain between the precipitates and the matrix as the precipitates coarsen and become incoherent or semicoherent.

THIS PAGE INTENTIONALLY LEFT BLANK

CONCLUSIONS

1. The critical quench rate for alloy 2090 is less than 46°C/s. Quench rates from 85°C/s to 46°C/s do not cause alloy 2090 to exhibit significantly different microstructures or tensile properties.

2. A slow quench rate results in the concurrent precipitation of T1 and delta prime. Precipitation of T1 along grain boundaries during slow cooling is the primary reason for the low mechanical properties after aging.

3. Unidentified grain boundary precipitates were observed in the slow quenched samples. It may be the equilibrium delta phase or metastable T2 phase.

REFERENCES

1. Preliminary data, NADC Round Robin, Report in Progress

2. Thompson, D.S., Subramanya, B.S., and Levy, S.A., Met. Trans., Vol.2, April 1971, p.1149

3. Conserva, M., and Fiorini, P., Met. Trans., Vol.4, March 1973, p.857

4. Smith, W.F., and Grant, N.J., Met. Trans., Vol.1, April 1970, p.979

5. Evancho, J.W., and Staley, J.T., Met Trans, Vol.5., Jan. 1974, p.43

6. Lorimer, G.W., "Precipitation in Aluminum Alloys", Precipitation in Solids, ed. Russel, K.C., Aaronson, H.I., (TMS Warrendale, PA, 1978) p.87

7. O'Dowd, M.E., Ruch, W., Starke E.A. Jr., Journal of Physics, Colloquium C3, supplement no.9, volume 48, September 1987, p.565.

THIS PAGE INTENTIONALLY LEFT BLANK

DISTRIBUTION LIST (Continued)
NADC-89046-60 No. of Copies

Naval Sea Systems Command 1
Washington, DC 20362

Office of Naval Technology 2
Washington, DC 20390
(2 copies for Code 225; ATTN: J. Kelly, M. Kinna)

Naval Air Development Center 12
Warminster, PA 18974-5000
(2 copies for Code 8131)
(10 copies for Code 6063; ATTN: M. Donnellan)

Naval Post Graduate School 1
Monterey, CA 93940
Attn: Dr. E. R. Wood (Code 67)

DISTRIBUTION LIST (Continued)
NADC-89046-60

No. of Copies

Naval Air Systems Command 4
Washington, DC 20361-0001
(1 copy for AIR-5304; ATTN: J. Collins)
(1 copy for AIR-931; ATTN: L. Sloter)
(2 copies for AIR-5004)

Annapolis Laboratory 1
David W. Taylor Naval Ship Research and
Development Center Detachment
Annapolis, MD 21402-1198

Naval Air Test Center 1
Patuxent River, MD 20670-5304

Naval Safety Center 1
MAS, Norfolk, VA 23511

Naval Research Laboratory 2
4555 Overlook Ave., SW
Washington, DC 20375
(1 copy for Code 6120)
(1 copy for Code 6306)

David W. Taylor Naval Ship Research and 1
Development Center
Bethesda, MD 20084-5000

Naval Ship Engineering Center 1
Washington, DC 20360
(1 copy for Code 6101E)

Naval Surface Weapons Center 1
Silver Spring, MD 20903
(1 copy for D. Divecha)

Defense Technical Information Center 2
ATTN. DTIC-FDAB
Cameron Station BG5
Alexandria, VA 22304-6145

Center for Naval Analysis 1
4401 Fort Avenue
P.O. Box 16268
Alexandria, VA 22302-0268

Office of Naval Research 1
Washington, DC 20350
(1 copy for Code 1131; ATTN: G. Yoder)